Modeling of swimming posture dynamics for a beaver-like robot

Gang Chen [a,b,*], Wang Peng [a], Zhenyu Wang [a], Jiajun Tu [c], Huosheng Hu [b], Donghai Wang [a,**], Hao Cheng [d], Lvyuan Zhu [e]

[a] School of Mechanical Engineering, Zhejiang Sci-Tech University, Hangzhou, 310018, China
[b] School of Computer Science and Electronic Engineering, University of Essex, Colchester, CO4 3SQ, UK
[c] Faculty of Intelligent Manufacturing, Jiaxing Vocational & Technical College, Jiaxing, 314000, China
[d] Zhejiang Institute of Industry and Information Technology, Hangzhou, 310000, China
[e] Zhejiang Manchinery Industry Federation, Hangzhou, 310009, China

A B S T R A C T

A bionic underwater robot swims to generate its propulsion in water, which in turn directly determines its movement stability. Exploring the relationship between the swimming force and the posture is important. This study aims to analyze and model the swimming posture dynamics of a beaver-like robot. The posture dynamics is decomposed into three parts: leg dynamics, body hydrodynamics, and body posture dynamics. First, the leg dynamic model of the beaver-like robot is established using the rigid-fluid integration method. Then, the overall fluid dynamics of the robot is modeled via numerical calculation methods to obtain the forces of the water on the robot body during swimming. Lastly, the swimming posture dynamic model of the robot is constructed to describe the relationship between the leg movement and body posture. The swimming process of the beaver-like robot with bionic alternating and synchronous trajectory is simulated with ADAMS 2019. The proposed modeling method and the swimming posture dynamic model are verified by comparing the simulation and theoretical calculation results of robot posture, which could be used for the swimming posture control of a bionic underwater robot.

Keywords:
Swimming posture dynamics Rigid-fluid integration dynamics Hydrodynamics Bionic underwater robot Beaver

1. Introduction

The ocean covers 70% of the Earth's total area and contains various narrow spaces, such as the cabin of shipwrecks, the cabin of crashed aircraft, underwater caves, trenches, submarine canyons, and hydrothermal vents. Underwater narrow-space exploration has important and far-reaching scientific value and significance for the study of life phenomena, processes, and laws in the ocean, the discovery of new mineral resources, and the development of rescue, salvage, and military applications. With the advancement in robotic technology, researchers have developed various bionic underwater robots for ocean exploration.

Chen et al. (2023b) used a neural network approach to model the movement of a soft-bodied robot fish. Nir et al. (2012) and Yu et al. (2016) studied and modeled the movement mechanism of fish and jellyfish. Chen et al. (2023a) designed a fish-inspired underwater vehicle with a wire-driven flexible spine and a servo motor-driven rigid caudal fin and used a dynamical approach to optimize swimming performance. Roper et al. (2011) studied the movement mechanism of turtles and crabs, which go forward by flapping; Richards and Clemente (2013) studied the movement mechanism of squid and jellyfish, which move by changing their cavities with water jets; Fan et al. (2017) studied the movement mechanism of frogs, which swim with webbed feet. Amphibians mostly move forward with their legs. Legs have multiple joints and webbed feet, which maintain high flexibility and propulsion efficiency. Different forms of amphibian-like robots have been developed. Wang et al. (2023) tested and analyzed the effect of leg structure parameters on swimming performance through hydrodynamic simulations and experiments. Chen et al. (2011) studied the movement mechanism and bionic mechanism synthesis of an amphibian-like turtle robot to implement motion mode switching in different environments. Gul et al. (2018) used multilayer 3D printing to build a soft frog robot with embedded shape-memory alloy and flex sensors.

The small space and complex terrain, often accompanied by variable currents, in an underwater narrow space put forward special

requirements to the robots for underwater narrow-space exploration. Such robots not only need to have the ability of agile swimming but also need to be able to work on the bottom of the sea. Existing bionic robots cannot effectively adapt to the requirements of underwater narrow-space exploration. Thus, a new type of underwater robot suitable for underwater narrow-space exploration should be developed. Through study of the biological structure and behavior of a beaver, we found that it possesses both mentioned qualities. The forelimbs of a beaver are flexible and can be used for seabed operation. The hind limbs are strong with webbed feet, a streamlined body, and a soft tail. The tail can provide a good balance of the body. These characteristics make beavers have good swimming performance and seabed operation ability. Inspired by beavers, this study combines the characteristics of underwater narrow-space exploration and the principle of bionics and proposes a beaver-like robot. It can be fully suitable and can effectively complete the exploration mission in underwater narrow space.

The beaver-like robot with webbed feet swims by paddling its legs to generate propulsion force. The stability of the robot's swimming posture directly affects the accuracy of underwater swimming trajectory. Its body flexibility is important to its underwater detection and operation performance. Based on fluid dynamic modeling and mechanical analysis of beavers, Chen et al. (2022) proposed a biological heuristic reinforcement learning control strategy. This method realizes the self-learning motion technique of a beaver-like robot. Takada et al. (2014b) established a computational simulation model of 3D fluid–structure interaction analysis of robotic fish. They conducted a hydrodynamic analysis of robotic fish (Takada et al., 2014a). Fujiwara and Yamaguchi (2017) developed and assessed a fish-like robot. Li et al. (2020) proposed a general multibody dynamic algorithm to solve various fish swimming problems, including a subpropulsion multi-degree of freedom (DOF) and rigid undulating body and an undulating body with multiple deformable fins. Richards and Christofer (2013) proposed a dynamic model of webbed paddling of a frog-like robot, which is suitable for various sizes and complex hydrodynamic problems, such as aquatic insects or fish fins. Research on the swimming dynamics of bionic underwater robots focused on the force analysis of one leg or part of the body instead of the overall study on the swimming posture dynamics of bionic underwater robots. Thus, the study of swimming posture dynamics for a beaver-like robot is necessary and significant.

In this study, a beaver-like robot is built with a set of locomotion mechanisms to achieve good swimming ability and to investigate the posture dynamics of the robot during swimming. Through constructing a hydrodynamic model of the robot, a rigid-liquid fusion method is used to establish a model of the overall dynamics of the beaver-like robot during swimming, and the relationship between leg movements and swimming posture is explained well. The correctness of the theory and model is verified through simulation and experiment, which provides a basis for realizing stable control of the posture of the underwater robot. The rest of this paper is organized as follows. In Section 2, the leg kinematic model of a beaver-like underwater robot is established. Section 3 analyzes the swimming posture dynamics of the beaver-like underwater robot. Simulations of the swimming posture dynamics of the robot are conducted in Section 4 to verify the dynamic model method. Swimming experiments are presented in Section 5. Finally, a brief conclusion and future work are given in Section 6.

2. Beaver-like underwater robot and kinematic model

2.1. Beaver-like underwater robot platform

A beaver is an amphibious mammal with a body length of about 80 cm. The tail is flattened and about 20 cm long. It has webbed hind limbs and is a good swimmer because of its several characteristics: 1. The beaver's powerful hind limbs allow it to swim very fast in the water. 2. The ability to bend and contract the forelimbs in swimming streamlines the body and reduces gliding resistance. 3. Compared with other amphibious robots, such as salamander-like robots, beaver-like robots require only one set of locomotion mechanisms, a design that reduces the complexity of the robots and increases the efficiency of movement. Based on the above advantages, we select a beaver as a bionic object.

Table 1
Dimensional parameters of the robot.

Components	Parameters	Numerical values	Materials
Forelimbs	Length of small arm (mm)	100	Resin
	Length of large arm (mm)	100	
Body	Total length (mm)	700	Resin
	Mass (kg)	4.2	
Hind limbs	Calf length (mm)	122	Resin
	Thigh length (mm)	100	
Webbed feet	First finger length (mm)	30	Resin and flexible silicone
	Second finger length (mm)	50	
	Size (mm^2)	10353	
Tail	Length (mm)	230	Double-layer flexible PVC material
	Size (mm^2)	18431	

The bionic robot designed in this study is about 70 cm long with a tail of 23 cm-long flexible plate. The parameters of the robot are shown in Table 1. The body of the bionic robot is basically the same as the beaver's structure, as illustrated in Fig. 1.

Based on a beaver, a beaver-like robot with extremely similar structure is designed. The robot is divided into five parts: forelimbs, body, hind limbs, webbed feet, and tail. The forelimbs are 3D printed with resin material, and all joints are replaced with motors. The forelimbs are contracted during movement to reduce water resistance. The body is a shell that is 3D printed with resin material and is streamlined. Electronic components are installed in the body and sealed. The parameters of the controller are shown in Table 2 and Fig. 2. The hind limb skeleton and toe of the webbed foot are 3D printed with resin material, and the webbed foot is further covered with soft silicone. In the forward motion process, the motor at the ankle drives the winding turntable to tighten the wire rope at the front of the palm and relax the wire rope at the palm to open the webbed foot to the maximum extent and maximize the propulsion. During the gliding phase, the motor at the ankle turns the winding reel in the opposite direction to loosen the wire rope at the front of the palm and tighten the wire rope at the center of the palm to fold the webbed foot and reduce water resistance. The details of the hind limb and webbed foot structure are shown in Fig. 3. The motor and sensor parameter information is presented in Table 3.

2.2. Kinematic model of a beaver-like underwater robot

2.2.1. Kinematic coordinate system

Fig. 4 shows the kinematic coordinate system of our beaver-like robot, which describes the motion (displacement and posture) of the robot in six DOFs while swimming. The displacement includes x, y, and z, which represent the forward, swing, and diving motion, respectively; the posture includes θ, φ, φ, which represent the pitch, heading, and roll motion, respectively.

Table 4 defines the relative symbolic variables of the pose, linear and angular velocities, force, and moment of the beaver-like underwater robot in the corresponding coordinate system. These variables are used to describe the changes in position and posture, linear and angular velocities, force, and torque during the robot's movement. η, ν, τ represent the posture, velocity/angular velocity, and force/torque of the robot under six DOFs, respectively, as shown in Eq. (1), Eq. (2), and Eq. (3) (Chen et al., 2021).

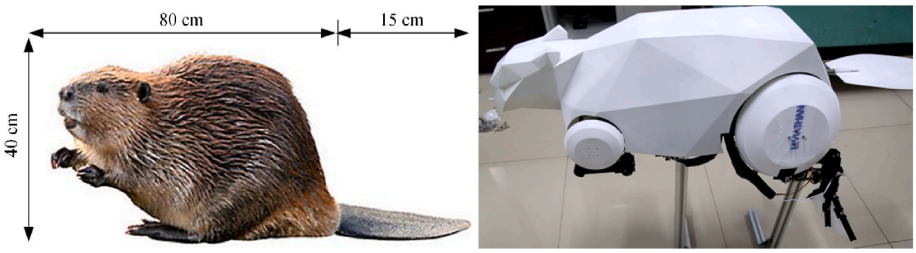

Fig. 1. Beaver prototype and robot platform.

Table 2
Parameters of the Arduino-based robot controller.

Parameters	Value
Type	ATmega328
Operating Voltage	5V
Pin DC Current (3.3V)	50 mA
I/O Pin DC Current	40 mA
Output Voltage	3.3V/5V

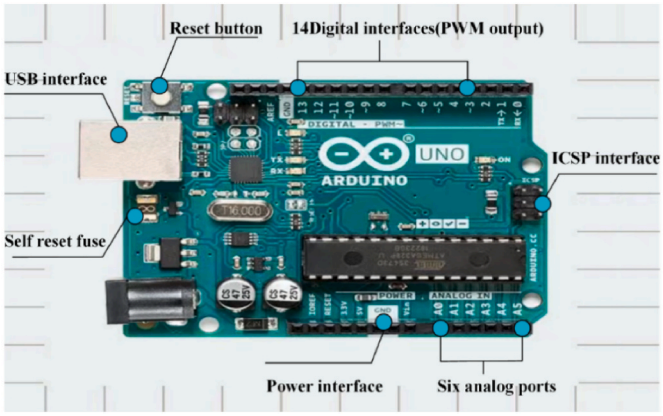

Fig. 2. Hardware diagram of the robot controller.

$$\eta = [x, y, z, \varphi, \theta, \varphi]^T \tag{1}$$

$$v = [u, v, w, p, q, r]^T \tag{2}$$

$$\tau = [X, Y, Z, K, M, N]^T \tag{3}$$

2.2.2. *Leg kinematic modeling*

Fig. 5 shows the leg kinematic model of the beaver-like robot, which has a total of three DOFs. This model transfers the velocity of body and leg movement to the end webbed foot, which is used to calculate the dynamic force generated in swimming. The leg linkage rotates around the Z-axis. The D-H parameters of the robot leg are shown in Table 5.

The position vector of the center of mass of each linkage rod is defined, as shown in Eq. (4), Eq. (5) and Eq. (6).

$${}^{1}p_{c_1} = l_1 \widehat{X}_1 \tag{4}$$

Table 3
Motor and sensor parameters.

Parameters	Motors in the forelimbs	Motors in the hind limbs	Motors in the tails	Posture sensors in body
Type	KM0950MD	DG-995MG	DG-995MG	BW-AH300
Voltage(V)-DC	5–6	4.8–6.0	4.8–6.0	9–35
Current (mA)	/	/	/	30–40
Torque (kg/cm)	33.8–4.5	15–17	15–17	/
Size (mm)	25*13*25	40*20*7	40*20*7	60*59*29
Mass(g)	13	58.8	58.8	150
Waterproof or not	Yes	Yes	Yes	IP67

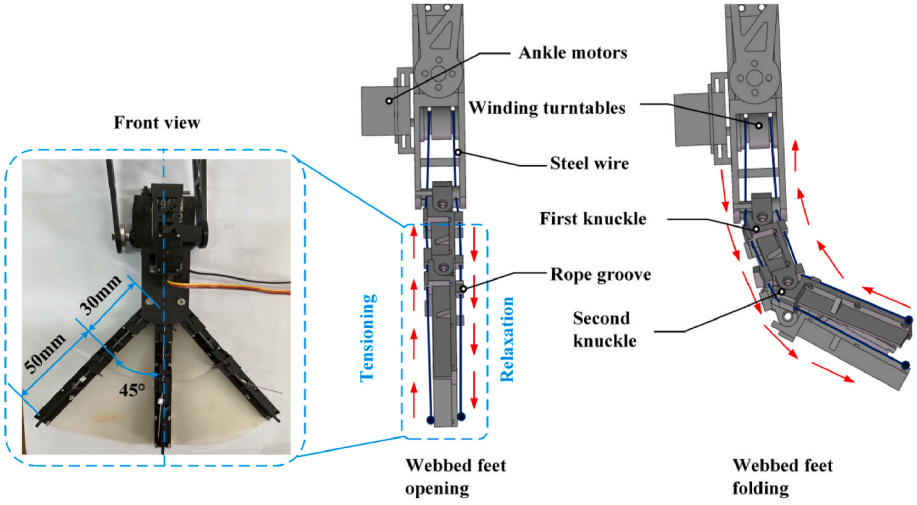

Fig. 3. Hind limb and webbed foot structure.

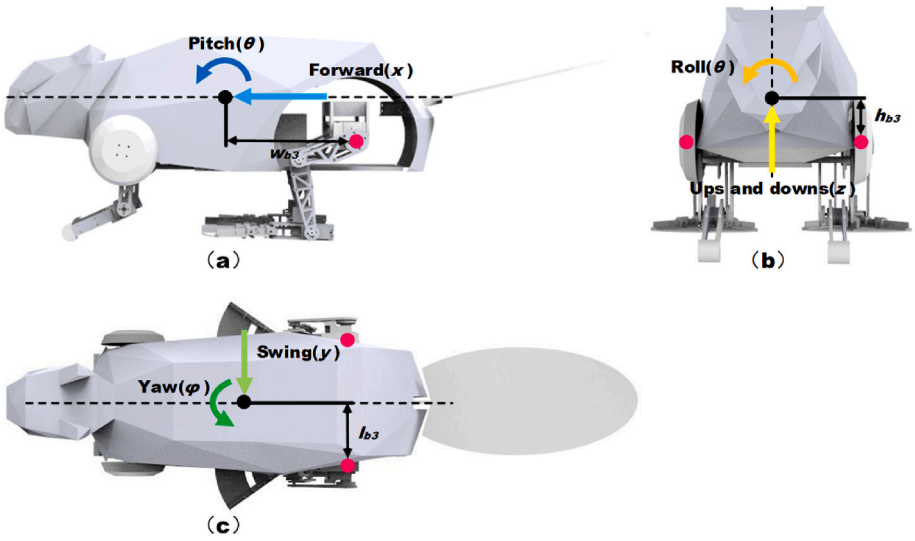

Fig. 4. Coordinate diagram of our beavers-like robot.

Table 4
Parameter definition of our beaver-like robot.

	Position and attitude	Linear velocity and angular velocity	Force and moment
Translation in the X direction (forward)	x	u	X
Translation in the Y direction (swing)	y	v	Y
Translation in the Z direction (ups and downs)	z	w	Z
Rotation about the X axis (roll)	φ	p	K
Rotation about the Y-axis (pitch)	θ	q	M
Rotation about the Z-axis (yaw)	φ	r	N

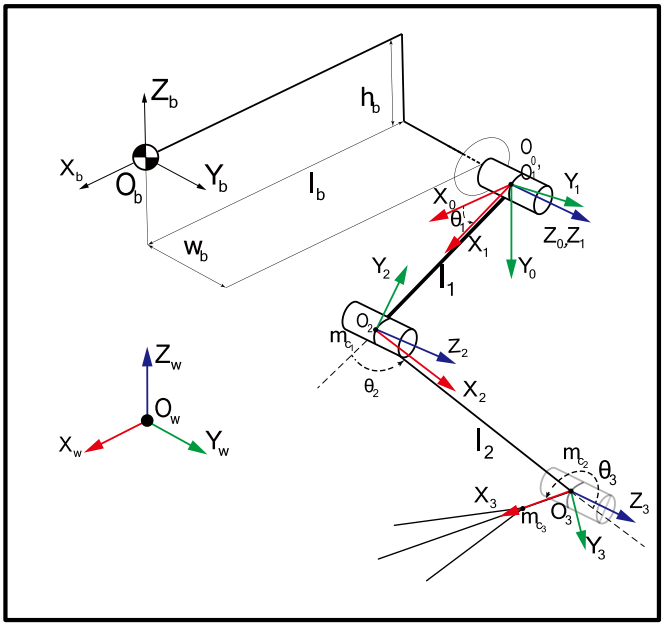

Fig. 5. Kinematic model of the leg of the beaver-like underwater robot.

Table 5
D-H parameters of the legs of the beaver-like underwater robot.

Jionts$_i$	α_{i-1}	a_{i-1}	d_i	θ_i
0	0	0	0	0
1	0	l_1	0	θ_1
2	0	l_2	0	θ_2
3	0	l_3	0	θ_3

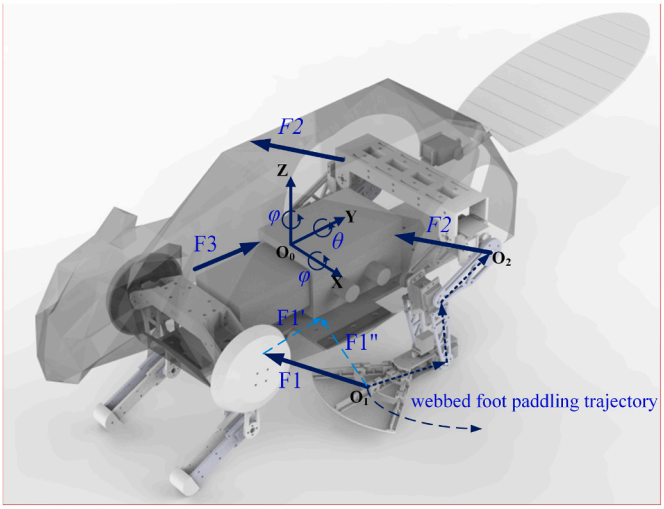

Fig. 6. Dynamic modeling schematic.

$$ {}^{2}p_{c_2} = l_2 \hat{X}_2 \tag{5} $$

$$ {}^{3}p_{c_3} = l_3 \hat{X}_3 \tag{6} $$

The material density of linkage is very low, and the relatively heavy motor is located at the joint so that the mass of linkage is concentrated at the joint. The inertia tensor of the center of mass of each linkage is 0 matrix, and the rotation matrix between adjacent coordinate systems is defined in Eq. (7), Eq. (8), and Eq. (9).

$$ {}^{1}_{0}R = \begin{bmatrix} c_1 & s_1 & 0 \\ -s_1 & c_1 & 0 \\ 0 & 0 & 1 \end{bmatrix} \tag{7} $$

$$ {}^{2}_{1}\mathrm{R} = \begin{bmatrix} c_2 & s_2 & 0 \\ -s_2 & c_2 & 0 \\ 0 & 0 & 1 \end{bmatrix} \tag{8} $$

$$ {}^{3}_{2}\mathrm{R} = \begin{bmatrix} c_3 & s_3 & 0 \\ -s_3 & c_3 & 0 \\ 0 & 0 & 1 \end{bmatrix} \tag{9} $$

3. Swimming posture dynamics of the beaver-like underwater robot

The dynamic modeling schematic is shown in Fig. 6. The modeling process for the swimming posture dynamics of the beaver-like robot is briefly described as follows:

Step.1: The hydrodynamics of the webbed foot is analyzed, and the hydrodynamic force F_1 is calculated (Chen et al., 2021).

Step.2: The force F_2 on the hip joint is calculated from F_1 by using the Newton–Euler iteration kinetic equation.

Step.3: On the basis of the data from fluid resistance F_3, hip joint force F_2, and posture, the relationship between the forces on the robot body and the change in posture is calculated. Afterward, the swimming posture dynamic model of the beaver-like underwater robot is constructed.

The parameters defined in Fig. 6 have the following meanings. O_0 is the absolute coordinate system of the robot's posture, O_1 is the force center at the webbed foot, and O_2 is the force center at the hip joint. F_1 is the propulsion generated by the webbed foot, F_2 is the force at the hip joint, and F_3 is the fluid resistance. φ is the posture angle of the robot body about the X-axis, θ is posture angle of the robot body about the Y-axis, and φ is the angle of rotation of the robot body about the Z-axis.

3.1. Dynamic modeling of legs

When a beaver-like robot swims in water, its leg joints rotate and actuate the webbed foot paddling, thus generating forward propulsion. The length of the thigh and calf linkages is l_1, l_2, respectively; the mass is m_1, m_2 respectively. The mass of the webbed foot is m_{c_1}, m_{c_2}, m_{c_3}. We define the body as joint 0, and its velocity and acceleration parameters are calculated using Eq. (10), Eq. (11), and Eq. (12).

$$ \omega_0 = 0 \tag{10} $$

$$ \dot{\omega}_0 = 0 \tag{11} $$

$$ {}^{0}\mathrm{v} = \begin{bmatrix} \mathrm{v}_{c_0} \\ 0 \\ 0 \end{bmatrix} \tag{12} $$

where v_{c_0} is the velocity at the center of mass.

$$ {}^{0}\dot{\mathrm{v}} = \begin{bmatrix} 0 \\ \mathrm{g} \\ 0 \end{bmatrix} \tag{13} $$

The hip joint is defined as joint 1. Its velocity and acceleration models are established using Eq. (14), Eq. (15), Eq. (16), Eq. (17), and Eq. (18).

$$ \omega_1 = {}^{1}_{0}\mathrm{R}\omega_0 + \dot{\theta}_1\hat{Z}_1 = \begin{bmatrix} 0 \\ 0 \\ \dot{\theta}_1 \end{bmatrix} \tag{14} $$

$$ \dot{\omega}_1 = {}^{1}_{0}\mathrm{R}\dot{\omega}_0 + {}^{1}_{0}\mathrm{R}\omega_0 \times \dot{\theta}_1\hat{Z}_1 + \ddot{\theta}_1\hat{Z}_1 = \begin{bmatrix} 0 \\ 0 \\ \ddot{\theta}_1 \end{bmatrix} \tag{15} $$

$$ {}^{1}\mathrm{v} = {}^{1}_{0}\mathrm{R}\left(\omega_0 \times \mathrm{P}_1 + {}^{0}\mathrm{v}\right) = \begin{bmatrix} \mathrm{v}_{c_0}\mathrm{c}_1 \\ -\mathrm{v}_{c_0}\mathrm{s}_1 \\ 0 \end{bmatrix} \tag{16} $$

$$ {}^{1}\dot{\mathrm{v}} = {}^{1}_{0}\mathrm{R}\left(\dot{\omega}_0 \times {}^{0}\mathrm{p} + \omega_0 \times \left(\omega_0 \times {}^{0}\mathrm{p}\right) + {}^{0}\dot{\mathrm{v}}\right) = \begin{bmatrix} \mathrm{gs}_1 \\ \mathrm{gc}_1 \\ 0 \end{bmatrix} \tag{17} $$

$$ \mathrm{v}_{c_1} = \dot{\omega}_1 \times {}^{1}\mathrm{P}_{c_1} + \omega_1 \times \left(\omega_1 \times {}^{1}\mathrm{P}_{c_1}\right) + {}^{1}\dot{\mathrm{v}}_1 = \begin{bmatrix} -\mathrm{l}_1\dot{\theta}_1^{\,2} + \mathrm{gs}_1 \\ \mathrm{l}_1\ddot{\theta}_1 + \mathrm{gc}_1 \\ \ddot{\theta}_1 \end{bmatrix} \tag{18} $$

The knee joint is defined as joint 2. Its velocity and acceleration models are established using Eq. (19), Eq. (20), Eq. (21), Eq. (22), and Eq. (23).

$$ \omega_2 = {}^{2}_{1}\mathrm{R}\omega_1 + \dot{\theta}_2\hat{Z}_2 = \begin{bmatrix} c_2 & s_2 & 0 \\ -s_2 & c_2 & 0 \\ 0 & 0 & 1 \end{bmatrix}\begin{bmatrix} 0 \\ 0 \\ \dot{\theta}_1 \end{bmatrix} + \begin{bmatrix} 0 \\ 0 \\ \dot{\theta}_2 \end{bmatrix} = \begin{bmatrix} 0 \\ 0 \\ \dot{\theta}_1 + \dot{\theta}_2 \end{bmatrix} \tag{19} $$

$$ \dot{\omega}_2 = {}^{2}_{1}\mathrm{R}\dot{\omega}_1 + {}^{2}_{1}\mathrm{R}\omega_1 \times \dot{\theta}_2\hat{Z}_2 + \ddot{\theta}_2\hat{Z}_2 = \begin{bmatrix} c_2 & s_2 & 0 \\ -s_2 & c_2 & 0 \\ 0 & 0 & 1 \end{bmatrix}\begin{bmatrix} 0 \\ 0 \\ \ddot{\theta}_1 \end{bmatrix} + \begin{bmatrix} 0 \\ 0 \\ \ddot{\theta}_2 \end{bmatrix} = \begin{bmatrix} 0 \\ 0 \\ \ddot{\theta}_1 + \ddot{\theta}_2 \end{bmatrix} \tag{20} $$

$$ {}^{2}\mathrm{v}_2 = {}^{2}_{1}\mathrm{R}\left(\omega_1 \times {}^{1}\mathrm{P}_2 + {}^{1}\mathrm{v}_1\right) = \begin{bmatrix} c_2 & s_2 & 0 \\ -s_2 & c_2 & 0 \\ 0 & 0 & 1 \end{bmatrix}\begin{bmatrix} \mathrm{v}_{c_0}\mathrm{c}_1 \\ -\mathrm{v}_{c_0}\mathrm{s}_1 \\ 0 \end{bmatrix} = \begin{bmatrix} \mathrm{v}_{c_0}\mathrm{c}_1\mathrm{c}_2 - \mathrm{v}_{c_0}\mathrm{s}_1\mathrm{s}_2 \\ -\mathrm{v}_{c_0}\mathrm{c}_1\mathrm{s}_2 - \mathrm{v}_{c_0}\mathrm{s}_1\mathrm{c}_2 \\ 0 \end{bmatrix} \tag{21} $$

$$ {}^{2}\dot{\mathrm{v}}_2 = {}^{2}_{1}\mathrm{R}\left(\dot{\omega}_1 \times {}^{1}\mathrm{p}_2 + \omega_1 \times \left(\omega_1 \times {}^{1}\mathrm{p}_2\right) + {}^{2}\dot{\mathrm{v}}_1\right) \tag{22} $$

$$ \mathrm{v}_{c_2} = \dot{\omega}_2 \times {}^{2}\mathrm{P}_{c_2} + \omega_2 \times \left(\omega_2 \times {}^{2}\mathrm{P}_{c_2}\right) + {}^{2}\dot{\mathrm{v}}_2 \tag{23} $$

The ankle joint is defined as joint 3. Its velocity and acceleration models are expressed by Eq. (24), Eq. (25), Eq. (26), Eq. (27), and Eq. (28).

$$ \omega_3 = {}^{3}_{2}\mathrm{R}\omega_2 + \dot{\theta}_3\hat{Z}_3 = \begin{bmatrix} c_3 & s_3 & 0 \\ -s_3 & c_3 & 0 \\ 0 & 0 & 1 \end{bmatrix}\begin{bmatrix} 0 \\ 0 \\ \dot{\theta}_1 + \dot{\theta}_2 \end{bmatrix} + \begin{bmatrix} 0 \\ 0 \\ \dot{\theta}_3 \end{bmatrix} \tag{24} $$

$$ \dot{\omega}_3 = {}^{3}_{2}\mathrm{R}\dot{\omega}_2 + {}^{3}_{2}\mathrm{R}\omega_2 \times \ddot{\theta}_3\hat{Z}_3 + \ddot{\theta}_3\hat{Z}_3 = \begin{bmatrix} 0 \\ 0 \\ \ddot{\theta}_1 + \ddot{\theta}_2 + \ddot{\theta}_3 \end{bmatrix} \tag{25} $$

$$ {}^{3}\mathrm{v}_3 = {}^{3}_{2}\mathrm{R}\left({}^{2}\omega_2 \times {}^{2}\mathrm{P}_3 + {}^{2}\mathrm{v}_2\right) \tag{26} $$

$$ {}^{3}\dot{\mathrm{v}}_3 = {}^{3}_{2}\mathrm{R}\left({}^{2}\dot{\mathrm{w}}_2 \times {}^{2}\mathrm{P}_3 + {}^{2}\omega_2 \times \left({}^{2}\omega_2 \times {}^{2}\mathrm{P}_3\right) + {}^{2}\dot{\mathrm{v}}_2\right) \tag{27} $$

$$ \dot{\mathrm{v}}_{c_3} = \dot{\omega}_3 \times {}^{2}\mathrm{P}_3 + \omega_3 \times \left(\omega_3 \times {}^{3}\mathrm{P}_{c_3}\right) + {}^{3}\dot{\mathrm{v}}_3 \tag{28} $$

${}^{0}f_w$ is the hydrodynamic force under fixed coordinates, which can be expressed by Eq. (29).

$$ {}^{0}\mathrm{f}_\mathrm{w} = \mathrm{C}^{*}\rho * \mathrm{A} * \mathrm{v}_{c_3} * \left|\mathrm{v}_{c_3}\right| \tag{29} $$

where C^* refers to the drag and lift coefficient (C_D, C_L) of the webbed foot, ρ is the density of water, and v_{c_3} is the velocity of the mass center of the foot.

The force on joint 3 is calculated using Eq. (30).

$$ {}^{3}\mathrm{f}_3 = {}^{3}\mathrm{f}_\mathrm{w} + {}^{3}\mathrm{F}_3 \tag{30} $$

where ${}^{3}F_3$ is the inertia force, which is expressed by Eq. (31).

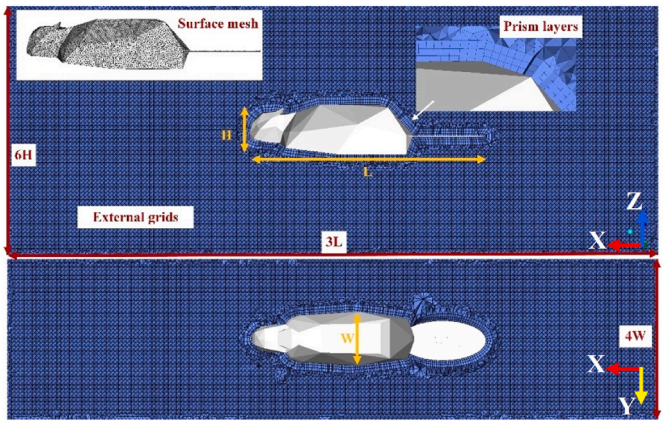

Fig. 7. Grid division of the body in the outflow field.

$$^{3}F_{3} = m_{c_3}\dot{v}_{c_3} \tag{31}$$

The torque on joint 3 is calculated using Eq. (32).

$$^{3}n_{3} = {}^{3}P_{c_3} \times \left({}^{3}F_{3} + {}^{3}f_{w}\right) \tag{32}$$

The forces and torque on the other joints are calculated using Eq. (33), Eq. (34), Eq. (35), Eq. (36), Eq. (37), and Eq. (38).

$$^{2}n_{2} = {}^{2}_{3}R\cdot{}^{3}n_{3} + {}^{3}p_{3} \times {}^{2}_{3}R\cdot{}^{3}F_{3} \tag{33}$$

$$^{2}F_{2} = {}^{2}_{3}R\cdot{}^{3}F_{3} + m_{2}\dot{v}_{2} \tag{34}$$

$$^{1}F_{1} = {}^{1}_{2}R\cdot{}^{2}F_{2} + m_{1}\dot{v}_{1} \tag{35}$$

$$^{0}n_{0} = {}^{0}_{1}R\cdot{}^{1}n_{1} \tag{36}$$

$$^{0}F_{0} = {}^{0}_{1}R\cdot{}^{1}F_{1} \tag{37}$$

$$^{0}F_{0} = {}^{0}_{1}R\cdot{}^{1}F_{1} \tag{38}$$

where $^{0}F_{0}$ and $^{0}n_{0}$ are the force and torque on the hip joint, respectively.

3.2. Force modeling of the robot body

The robot body is subject to water fluid force during robot swimming. The force is determined by the flow field which is generated by the interaction between the swimming robot and water and is difficult to model by theoretical calculation and experiments. Here we use the fluid simulation to model the fluid force on the robot body with computational fluid dynamic software.

To calculate the forces on the robot body in water, a robot body model is introduced into the Fluent fluid simulation software to hold the robot body stationary and simulate the drag and lift forces on the shell for different fluid velocity impacts. The forces on the robot body are measured in the range of fluid velocities of 0–1 m/s, and then a second-order polynomial is used to fit the relationship between the velocity and the robot forces in the water.

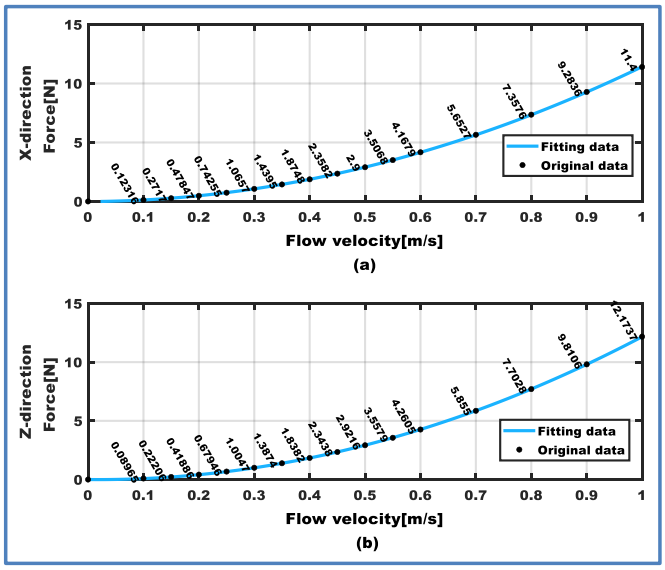

Fig. 9. Force on the body in the X and Z direction in fluid simulation.

3.2.1. Grid generation of the body in the fluid simulation

The grid generation is shown in Fig. 7. The outflow field is automatically divided by tetrahedral grid, and three prismatic layers are added at the interface of the body surface to improve the calculation accuracy.

The static approach is used in Fluent to simulate the robot's swimming state at different velocities. The robot's swimming state at different speeds is simulated by setting different water velocities. The environment setup and simulation process are as follows.

(1) The robot is directly set in front of the water velocity inflow port, the flow velocity is set to a fixed value, and the flow outlet is set to a pressure value.
(2) When a simulation reaches steady state, the lift and drag forces on the robot at that velocity are obtained, i.e., the lift and drag forces on the robot are obtained when it is moving at that velocity. The simulation simulates the drag and lift forces on the robot at different flow velocities from 0 to 1 m/s with an interval of 0.1 m/s.
(3) Finally, the continuous functions of the robot's swimming velocity and lift and drag forces are approximated with a second-order polynomial fitting.

3.2.2. Force model of the body with fluid simulation results

Fig. 8 shows the flow velocity clouds for each part of the robot's body

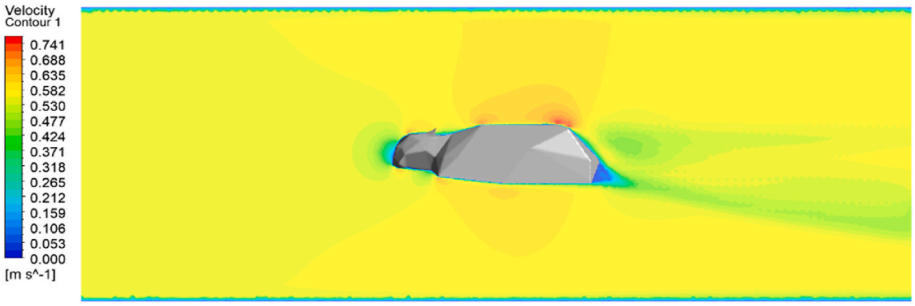

Fig. 8. Flow velocity cloud diagram of the outflow field.

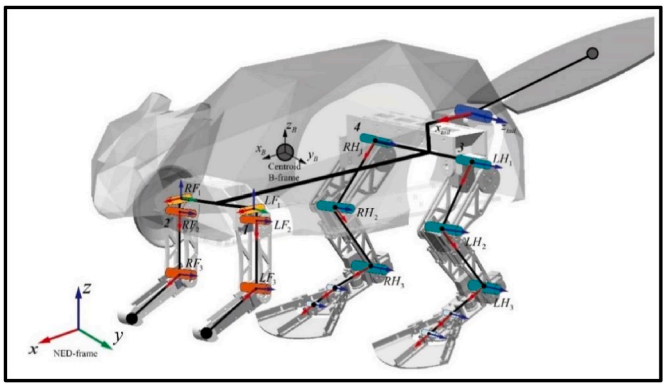

Fig. 10. Overall D-H parameters of the beaver-like robot.

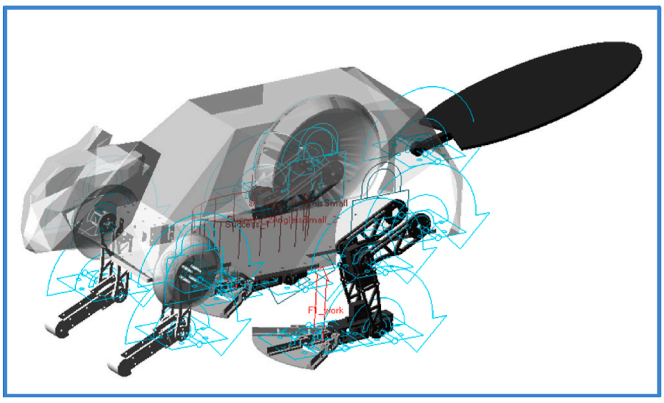

Fig. 11. ADAMS simulation model of our beaver-like robot.

under the flow velocity of 0.5 m/s. The head and tail are subjected to larger forces and smaller fluid velocities. The rest of the body is streamlined and subjected to smaller forces and larger fluid velocities. Fig. 9 presents the variation curves of the X- and Z-axis forces on the robot's body by setting different flow velocities in the simulation environment fluid.

The forces on the X- and Z-axis of the robot body are obtained by setting different fluid velocities for discrete simulations. Eq. (39) and Eq. (40) are obtained by fitting a second-order polynomial based on the discrete data of fluid velocity and force. Then, the relationship between the velocity and the forces on the robot in the swimming state is obtained.

$$F_{kx} = 11.2v^2 + 0.2v \tag{39}$$

$$F_{kz} = 12.6v^2 - 0.5v \tag{40}$$

where v is the velocity of the fluid.

3.3. Dynamic modeling of the swimming posture of the beaver-like underwater robot

Newton–Euler equations are used to model the dynamics of webbed foot, leg, tail, and whole body of the robot. Fig. 10 shows the coordinate system of the robot, namely, the global coordinate system {W} and the body coordinate system {B}.

The inertial matrix M_{RB} of the robot can be obtained using Eq. (41).

$$\mathrm{M_{RB}} = \begin{bmatrix} 4.35 & 0 & 0 & 0 & 0 & 0 \\ 0 & 4.35 & 0 & 0 & 0 & 0 \\ 0 & 0 & 4.35 & 0 & 0 & 0 \\ 0 & 0 & 0 & 0.21 & 0 & 0.0015 \\ 0 & 0 & 0 & 0 & 0.28 & 0 \\ 0 & 0 & 0 & 0.0019 & 0 & 0.32 \end{bmatrix} \tag{41}$$

In consideration of the low swimming velocity of the robot, the inertia matrix can be simplified as Eq. (42).

$$\mathrm{M_{RB}} = \mathrm{diag}\{[4.35\ 4.35\ 4.35\ 0.21\ 0.28\ 0.32]\} \tag{42}$$

The coordinate point of leg 3 in the motion coordinate system $X_BY_BZ_B$ (body) is expressed by Eq. (43).

$$\mathrm{P_3} = \begin{bmatrix} \mathrm{l_b} \\ \mathrm{h_b} \\ \mathrm{w_b} \end{bmatrix} \tag{43}$$

Then, the force/moment of the single hip joint on the center of mass of the body is $F_0 \times P_3 + n_0$ and F_0. The coordinate point of the corresponding joint in leg 4 is expressed by Eq. (44).

$$\mathrm{P_4} = \begin{bmatrix} \mathrm{l_b} \\ -\mathrm{h_b} \\ \mathrm{w_b} \end{bmatrix} \tag{44}$$

The force/moment at the center of mass of hip joints 3 and 4 is τ_{hip}, which is calculated using Eq. (45).

$$\tau_{\mathrm{hip}} = \begin{pmatrix} \mathrm{F_{(4)0}} + \mathrm{F_{(3)0}} \\ 0^{1\times 3} \end{pmatrix} + \begin{pmatrix} 0^{1\times 3} \\ \mathrm{F_{(4)0}} \times \mathrm{p_4} + \mathrm{F_{(3)0}} \times \mathrm{p_3} + {}^{0}\mathrm{n_{(3)0}} + {}^{0}\mathrm{n_{(4)0}} \end{pmatrix} \tag{45}$$

where $F_{(4)0}$ and $F_{(3)0}$ are related to both the posture of the leg joints and the velocity of the webbed foot at that moment.

According to the force model of the body, the comprehensive hydrodynamic force received by the underwater robot while swimming is calculated using Eq. (46).

$$\tau_{\mathrm{shell}} = \begin{bmatrix} \mathrm{F_{kx}} \\ \mathrm{F_{ky}} \\ \mathrm{F_{kz}} \end{bmatrix} = \begin{bmatrix} 11.2\mathrm{v}^2 + 0.2\mathrm{v} \\ 0 \\ 12.6\mathrm{v}^2 - 0.5\mathrm{v} \end{bmatrix} \tag{46}$$

Then, the resultant force/torque of the robot's body in the swimming state is calculated using Eq. (47).

$$\tau = \tau_{\mathrm{shell}} + \tau_{\mathrm{hip}} \tag{47}$$

Thus, the posture dynamic model of the robot in the swimming state can be obtained using Eq. (48).

$$\mathrm{M_{RB}} \bullet \dot{\mathrm{v}}_{(\mathrm{t})} = \tau \tag{48}$$

Furthermore, the swimming posture of the robot can be obtained using Eq. (49), Eq. (50), and Eq. (51).

$$\dot{\mathrm{v}}_{(\mathrm{t})} = \mathrm{M_{RB}^{-1}}\tau \tag{49}$$

$$\mathrm{v}_{(\mathrm{t})} = \int \left(\mathrm{M_{RB}^{-1}}\tau\right)\mathrm{dt} \tag{50}$$

$$\eta_{(t)} = \int\int \left(M_{RB}^{-1}\tau\right)\, dt \tag{51}$$

4. Simulation of the swimming posture dynamic model of the beaver-like underwater robot

Fig. 11 shows a beaver-like robot prototype model established in ADAMS. The paddling force of the webbed foot and the fluid force on the body obtained through Fluent simulation are added to the ADAMS model. The two motion modes of the robot, namely, alternating and synchronous swimming, are simulated to obtain the torques of the hip, knee, and ankle joint and the posture (pitch, yaw, and roll) of the robot in the process of moving forward. Then, the results are compared with those obtained by theoretical modeling in MATLAB to verify the

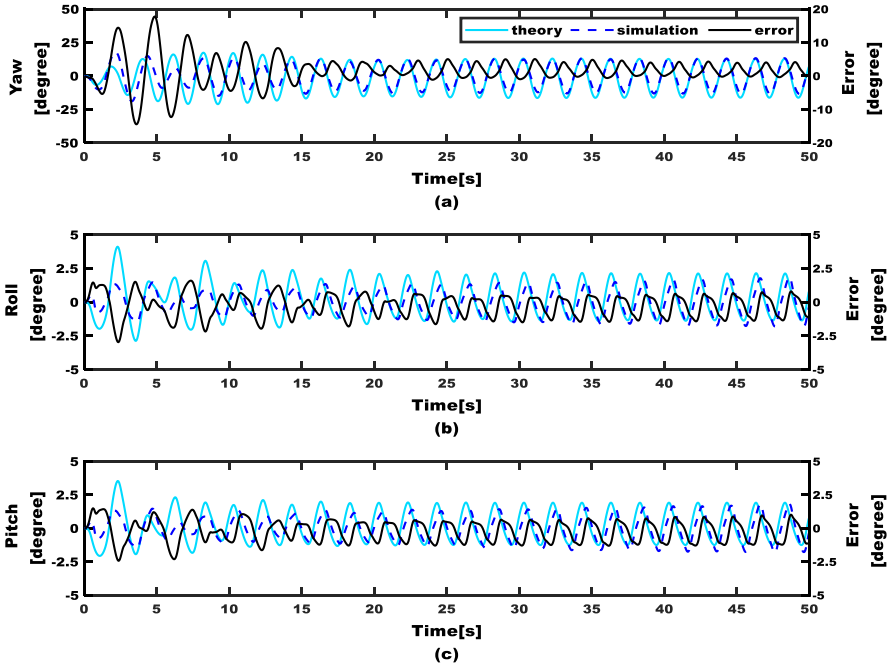

Fig. 12. Posture of the beaver-like underwater robot in alternate swimming mode.

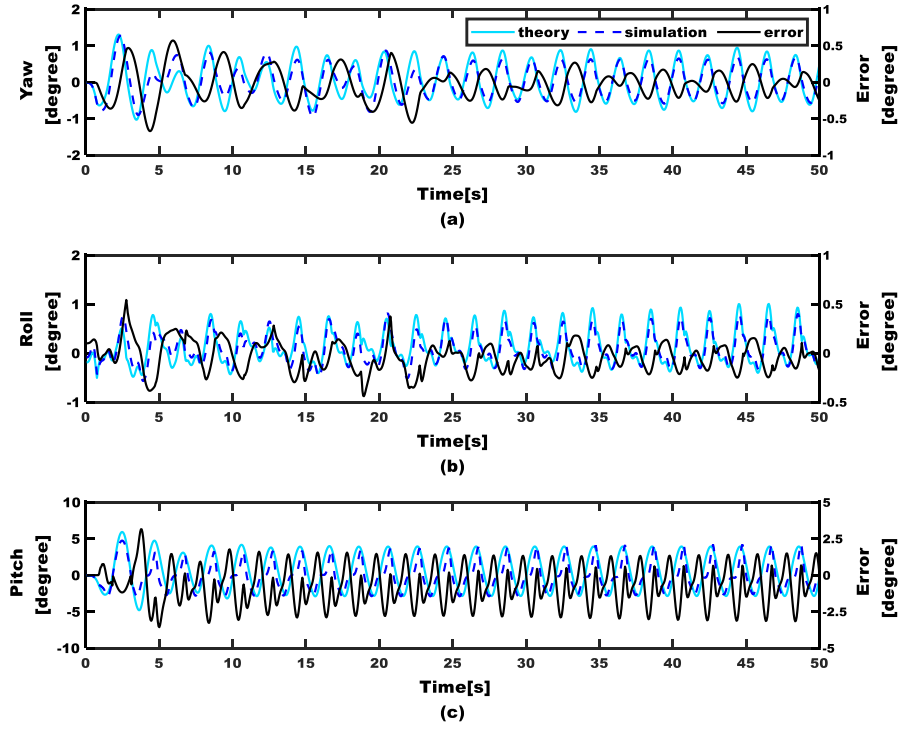

Fig. 13. Attitude change curve of the beaver-like underwater robot in synchronous swimming mode.

correctness of the swimming posture dynamic modeling of the robot.

Fig. 12 shows the posture changes with the alternate swimming mode of the beaver-like robot. In the first 10 seconds, the robot posture errors between the theoretical and simulation results fluctuate greatly, and the errors reach the peak value of 18° in the yaw direction. The main reasons for this phenomenon are as follows. When the robot initially moves from a static state, the fluid resistance has a rapid nonlinear change in a short time, which cannot be accurately computed in the theoretical model. After several cycles of motion, the hydrodynamic force generated by the webbed foot paddling and the additional mass force and resistance reach a relatively stable state. The attitude error is maintained stably in the range of 0–5°. The trend of posture in the roll

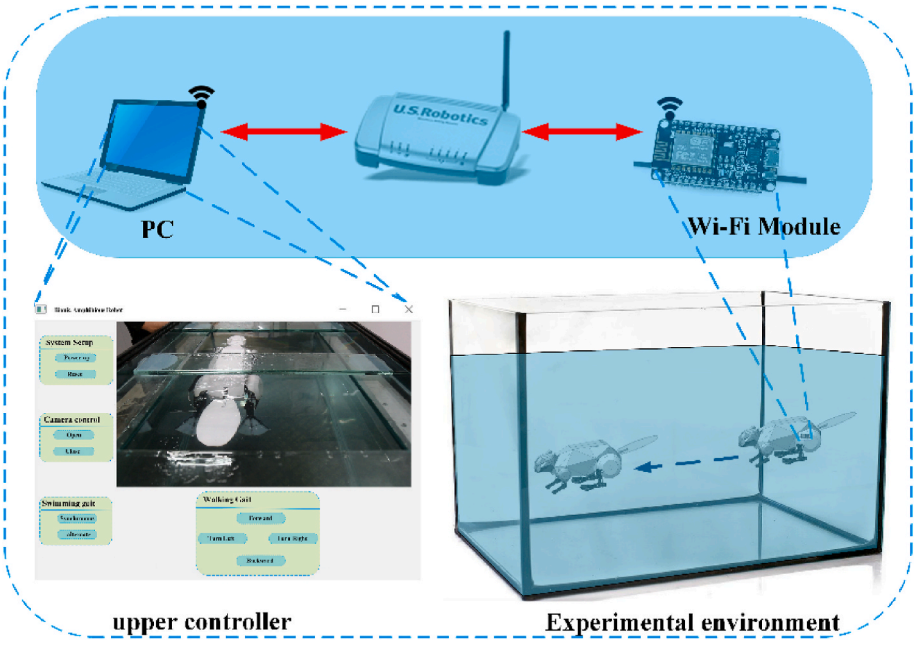

Fig. 14. Control structure in the experiment.

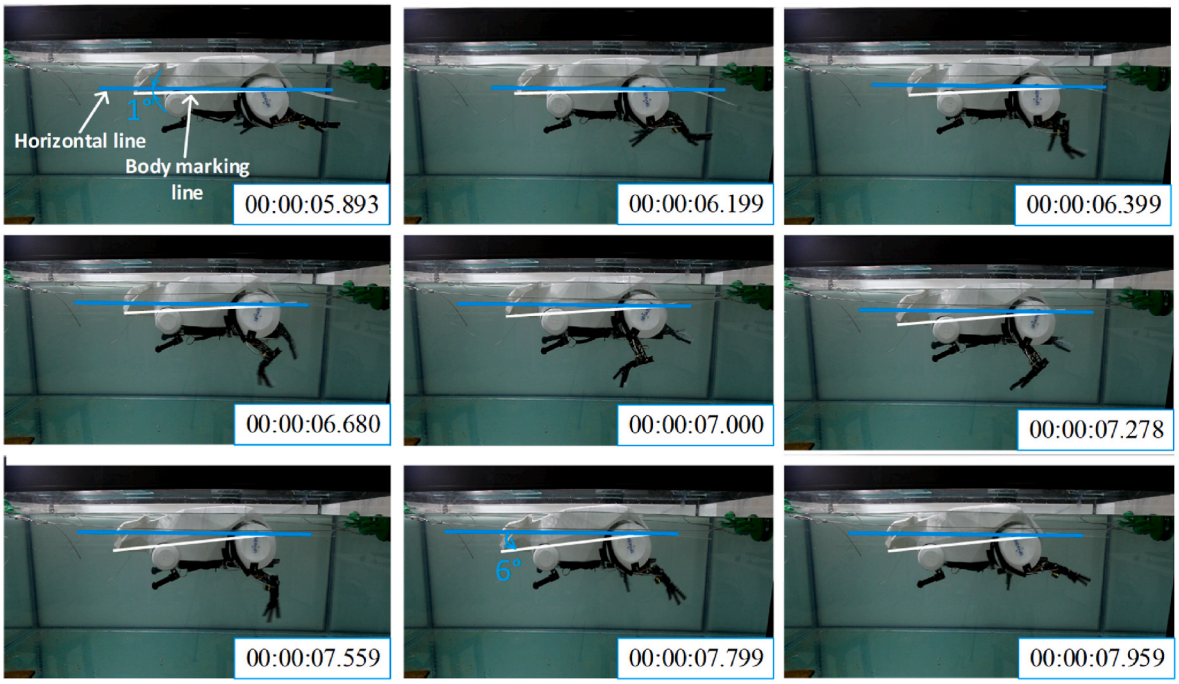

Fig. 15. Alternate swimming experiment of our beaver-like robot.

and pitch directions is similar to the posture in the yaw direction, and their amplitude changes are small because the hydrodynamic forces generated by the two with alternate paddling webbed feet partly cancel each other out.

Fig. 13(a) and (b) show that the posture amplitudes in the yaw and roll directions change minimally because the hydrodynamic forces generated by the webbed feet with synchronous paddling partly cancel each other out in the synchronous motion of the robot. In the pitch direction, a relatively moment is generated because of the synchronous paddling of the webbed feet. Thus, the change in pitch amplitude reaches 7°, but it is smaller than that in yaw amplitude. The reason is that the rotational inertia in the pitch direction is larger than that in the yaw direction.

5. Swimming experiments of the beaver-like robot

In the swimming experiments, the beaver-like robot is powered directly via a power cable and communicates with the upper controller running on a PC via the VNC Connect software in the same LAN. In detail, the upper controller sends the motion instructions to the robot and collects the posture dada of the robot. The robot controls the motors in accordance with the motion instructions from the upper controller and provides the motion states to the upper controller. The control structure diagram is shown in Fig. 14.

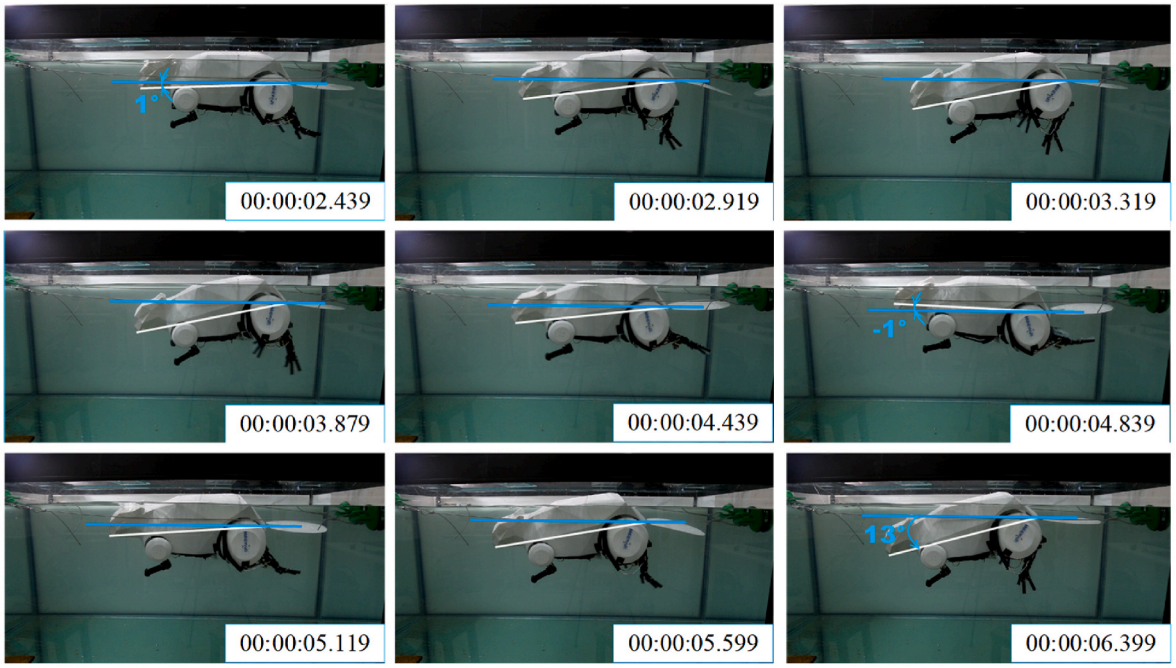

Fig. 16. Synchronous swimming experiments of our beaver-like robot.

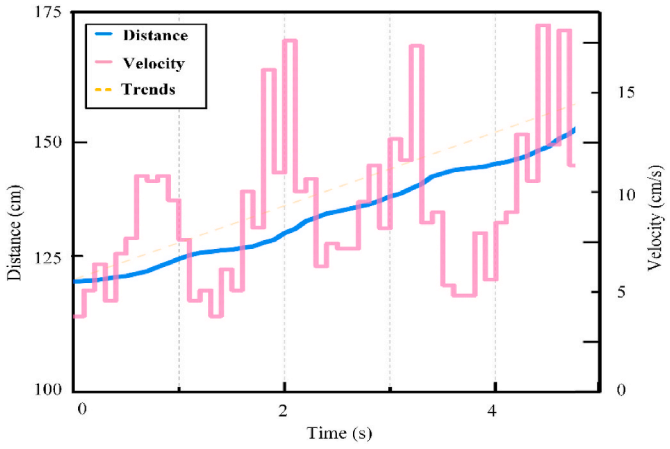

Fig. 17. Velocity and displacement in the alternate swimming mode.

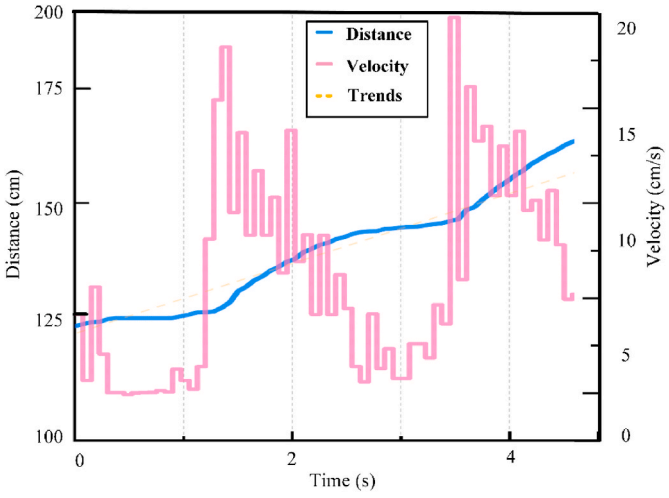

Fig. 18. Velocity and displacement in the synchronous swimming mode.

Figs. 15 and 16 show the movement process of the beaver-like underwater robot with alternate and synchronous swimming modes, respectively. In alternate swimming, the two hind limbs of the robot propel the body forward by alternate paddling. In one movement cycle, the two webbed feet provide propulsion force alternately, so that the body can move continuously. The movement process is relatively stable, and the pitch angle does not change considerably, maintaining in the range of 1°–6°. In synchronous swimming, the two hind limbs of the robot move forward synchronously. In one movement cycle, the two webbed feet provide propulsion force and withstand the resistance of water flow at the same time. Given that the propulsion force is not continuous, the movement process is not smooth, and the pitch angle changes greatly, reaching 13°. Through the experiments of alternate and synchronous swimming, the characteristics of posture change in different swimming modes of the robot are verified, and the necessity of the dynamic analysis of swimming posture and the correctness of the model are demonstrated.

As shown in Fig. 17, the maximum swim velocity is 0.204 m/s, which is about 0.292 BL/s (body length per second); the average speed is 0.075 m/s, which is about 0.119 BL/s. From Fig. 18, the maximum swim velocity is 0.160 m/s, which is about 0.229 BL/s; the average speed is 0.052 m/s, which is about 0.074 BL/s.

Table 6
Parameters of bionic robots.

Serial number	Dimension (mm)	Mass (kg)	Frequency (Hz)
1	**700*258*360**	**4.2**	**0.5**
2	680*200*80	7.76	0.5
3	320*560	3.8	0.8
4	495*50*80	1.29	1.91
5	900*500	3.73	0.5
6	530*373*165	3.4	0.5
7	710*640*42	4.7	1.11

According to the research on the swimming performance of various types of underwater robots, we can obtain a table of the parameters of various types of bionic underwater robots and a comparison chart of

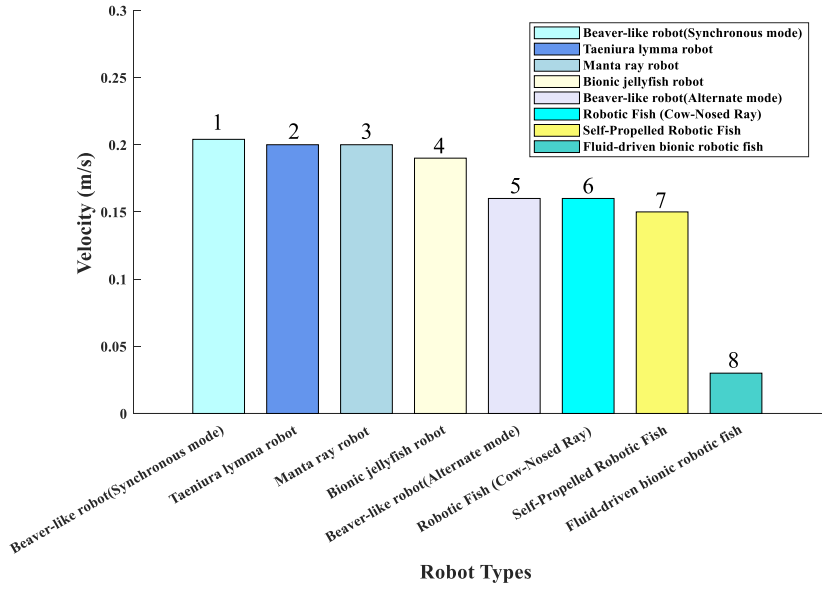

Fig. 19. Swimming velocity of underwater bionic robots.
1- (Beaver-like robot) 2- (Zhang and Jianhui He, 2012) 3- (Huang et al., 2021) 4- (Li, He et al., 2023).
5- (Beaver-like robot) 6- (Cai et al., 2010) 7- (Wu et al., 2014) 8- (Xia et al., 2023).

robot swimming speed, as shown in Table 6 and Fig. 19, respectively. The information in Fig. 19 and Table 6 indicates that the beaver-like robot has an advantage in swimming speed when the robots have a similar form factor, minimal difference in mass, and the same motion frequency.

6. Conclusions

In this study, the characteristics of a beaver are discussed and imitated. A beaver-like robot is designed with a set of locomotion mechanisms, and the swimming posture dynamics of the robot is investigated. A rigid-liquid fusion method is used to establish a model of the overall dynamics of the beaver-like robot while swimming, and the relationship between leg movements and swimming posture is explained in detail. This provides a basis for realizing stable posture control of the underwater robot. The main conclusions are provided below.

First, a beaver-like robot is designed in accordance with the shape and skeletal characteristics of a beaver. The robot structure includes five parts: forelimbs, body, hind limbs, webbed feet, and tail. The webbed feet can realize alternate and synchronous swimming. The body shell adopts a streamlined shape to reduce water resistance. The webbed feet are rope-driven to extend and contract and coordinate with the hind limbs for increasing the propulsion and reducing the resistance force while swimming.

Through dynamic modeling, hydrodynamic models of the webbed feet, hind limbs, and posture of the beaver-like robot are constructed, and the relationship between the force on the robot and the posture is determined. The correctness and rationality of the modeling method are verified through simulation and experiment.

From the calculation results of the simulation model, the change in robot body posture is basically the same when the robot moves with alternate and synchronous swimming modes stably. The maximum errors of yaw, roll, and pitch are 4.46°, 1.59°, and 1.50°, respectively, when the feet move alternately. Meanwhile, the maximum errors of yaw, roll, and pitch are 0.54°, 0.54°, and 3.15°, respectively, when the feet move synchronously. These results can verify the correctness and validity of the swimming posture dynamic modeling method.

According to the comparison of the velocity and displacement curves of alternate and synchronous swimming, the maximum velocity is 0.204 m/s and the maximum pitch angle change is 13° during synchronous swimming. During alternate swimming, the maximum velocity is 0.160 m/s, and the maximum pitch angle change is 6°. From the comparison of the characteristics of different swimming modes, we can learn that stable posture control of the underwater robot can be achieved by flexibly adopting two different swimming modes in the complicated underwater environment.

In the future work, we will add artificial skin to the body surface so that the robot can adapt well to a real environment and realize enhanced swimming performance. Autonomous swimming will also be studied with decreased remote wireless control to improve the robot's intelligence. Moreover, the swimming efficiency of the beaver-like robot will be evaluated further, and accurate calculation and verification will be carried out for the work done by the component force of the beaver-like robot in the swimming process.

Acknowledgements

This work was financially supported by National Natural Science Foundation of China (Nos. 52275037, 51875528, and 41506116), the Key Research and Development Project of Zhejiang Province (No. 2023C03015), Zhejiang Provincial Natural Science Foundation of China (Nos. LY20E050018 and LTY21F030001), and Science Foundation of Zhejiang Sci-Tech University (ZSTU) (No. 17022183-Y).

References

Cai, Yueri, Bi, Shusheng, Zheng, Licheng, 2010. Design and experiments of a robotic fish imitating cow-nosed ray. JBE. ISSN: 1672-6529 7 (Issue 2), 120–126.

Chen, Xuedong, 2011. Research on motion mechanism and biomimetic mechanism synthesis of amphibious biomimetic turtle robot in multi-medium environment. J. Mech. Eng. 47 (2) (in Chinese), 2011:197-197.

Chen, Gang, Tu, Jiajun, Ti, Xiaocong, Wang, Zhenyu, Hu, Huosheng, 2021. Hydrodynamic model of the beaver-like bendable webbed foot and paddling characteristics under different flow velocities. Ocean Eng. 234, 109179.

Chen, Gang, Lu, Yuwang, Yang, Xin, Hu, Huosheng, 2022. Reinforcement learning control for the swimming motions of a beaver-like, single-legged robot based on biological inspiration [J]. Robot. Autonom. Syst. 154, 1–12.

Chen, Gang, Zhao, Zhihan, Wang, Zhenyu, Tu, Jiajun, Hu, Huosheng, 2023a. [J]. Ocean Eng. 271, 113748.

Chen, Gang, Yang, Xin, Xu, Yidong, Lu, Yuwang, Hu, Huosheng, 2023b. Neural network-based motion modeling and control of water-actuated soft robotic fish [J]. Smart Mater. Struct. 32 (1), 015004.

Fujiwara, Shinpei, Yamaguchi, Satoru, 2017. Development of fishlike robot that imitates carangiform and subcarangiform swimming motions. J. Aero Aqua Bio-mech. 1–8.

Huang, Haocai, Sheng, Chaowu, Wu, Jiannan, Wu, Gang, Zhou, Chunlin, Wang, Hangzhou, 2021. Hydrodynamic analysis and motion simulation of fin and propeller driven manta ray robot. Appl. Ocean Res. 108, 102528.

Jizhuang, Fan., Wei, Zhang., Bowen, Yuan., Gangfeng, Liu., 2017. Propulsive efficiency of frog swimming with different feet and swimming patterns. Biol. Open 503–510.

Richards, Christopher T. and Christofer J. Clemente. “Built for rowing: frog muscle is tuned to limb morphology to power swimming.” Journal of The Royal Society Interface 10 (2013): n. pag.

Li He, Wang, Guanzhong, Li, Longjie, Wei, Minyu, Li, Yuanbo, Sun, Wei, Zeng, Qingliang, 2023. Design of the swimming system of a bionic jellyfish robot for seabed exploration. Appl. Ocean Res. 134, 103498.

Li, Ruoxin, Xiao, Qing, Liu, Yuanchuan, Li, Lijun, Liu, Hao, 2020. Computational investigation on a self-propelled pufferfish driven by multiple fins. Ocean Eng., 106908

Nir, S., Ruchaevski, I., Shraga, S., Shteinberg, T., Ben, Moshe, 2012. A Jellyfish-like robot for mimicking jet propulsion. In: 2012 IEEE 27th Convention of Electrical and Electronics Engineers in Israel, pp. 1–5.

Richards, C.T., Clemente, C.J., 2013. Built for rowing: frog muscle is tuned to limb morphology to power swimming. J. Roy. Soc. Interface 10.

Roper, D.T., Sharma, S., Sutton, R., Culverhouse, P., 2011. A review of developments towards biologically inspired propulsion systems for autonomous underwater vehicles. In: Proceedings of the Institution of Mechanical Engineers, Part M: Journal of Engineering for the Maritime Environment, pp. 77–96.

Jahan Zeb, Gul, Sajid, Memoon, Rehman, Muhammad Muqeet, Siddiqui, Ghayas Uddin, Shah, Imran, Kyung-Hwan, Kim, Jae, Wook Lee, Hyun Choi, Kyung, 2018. 3D printing for soft robotics – a review. Sci. Technol. Adv. Mater. 243–262.

Takada, Yogo, Koyama, Keisuke, Usami, Takahiro, 2014a. Robotic fish. J. Robot. Mechatron. 391–393.

Takada, Yogo, Ochiai, Toshinori, Fukuzaki, Noboru, Tajiri, Tomoki, Wakisaka, Tomoyuki, 2014b. Analysis of flow around robotic fish by three-dimensional fluid-structure interaction simulation and evaluation of propulsive performance. J. Aero Aqua Bio-Mech. 57–64.

Wang, Gang, Liu, Kaixin, Ma, Xinmeng, Chen, Xi, Hu, Shihao, Tang, Qinyun, Liu, Zhaojin, Ding, Mingxuan, 2023. Songjie Han,Optimal design and implementation of an amphibious bionic legged robot. Ocean Eng. 272, 113823.

Wu, Zhengxing, Yu, Junzhi, Tan, Min, Zhang, Jianwei, 2014. Kinematic comparison of forward and backward swimming and maneuvering in a self-propelled sub-carangiform robotic fish. JBE 11 (Issue 2), 199–212.

Xia, Qingchao, Hong, Li, Song, Nan, Wu, Zeliang, Wang, Xiang, Sun, Xu, Zhang, Sheng, Yang, Canjun, 2023. Research on flexible collapsible fluid-driven bionic robotic fish. Ocean Eng. 276, 114203.

Yu, J., Yuan, J., Wu, Z., Tan, M., 2016. Data-driven dynamic modeling for a swimming robotic fish. IEEE Trans. Ind. Electron. 5632–5640.

Zhang, Yonghua, Jianhui He, K.H., 2012. Low,Parametric study of an underwater finned propulsor inspired by bluespotted ray. JBE 9 (Issue 2), 166–176.